Enhanced antibacterial activity through silver nanoparticles deposited onto carboxylated graphene oxide surface

Arturo Barjola
Universitat Politècnica de València: Universitat Politecnica de Valencia
María Ángeles Tormo
Hospital La Fe Investigation Centre: Instituto de Investigacion Sanitaria La Fe
Oscar Sahuquillo
Universitat Politècnica de València: Universitat Politecnica de Valencia
Patricia Bernabé
Hospital La Fe Investigation Centre: Instituto de Investigacion Sanitaria La Fe
José Manuel Pérez
Hospital La Fe Investigation Centre: Instituto de Investigacion Sanitaria La Fe
Enrique Gimenez (enrique.gimenez@mcm.upv.es)
Universitat Politècnica de València (UPV) https://orcid.org/0000-0002-6330-0209

Nano Express

Keywords: carboxylated graphene oxide, antimicrobial, biocide, silver-nanoparticles

Posted Date: November 1st, 2021

DOI: https://doi.org/10.21203/rs.3.rs-996008/v1

Abstract

The strong bactericidal action of silver nanoparticles (AgNPs) is usually limited for their degree of aggregation. Deposition of AgNPs onto a graphene oxide (GO) surface to generate GO-Ag hybrids has been shown to be an effective method to control these aggregation problems. In this sense, a novel carboxylated graphene oxide-silver nanoparticle (GOCOOH-Ag) material has been synthesized and their antibacterial and biofilm formation inhibition have been studied.

AgNPs decorating the GOCOOH surface achieved an average size of 6.74±0.25 nm, which was smaller than those of AgNPs deposited onto the GO surface. In addition, better distribution of AgNPs was obtained using carboxylated material. It is important to highlight the main role of the carboxylic groups in the nucleation and growth of the AgNPs that decorate the GO-based material surface.

In vitro antibacterial activity and antibiofilm-forming action were tested against Gram-positive (*Staphylococcus aureus* and *Staphylococcus epidermidis*) and Gram-negative bacteria (*Pseudomonas aeruginosa* and *Escherichia coli*). Both GO-Ag and GOCOOH-Ag reduced the bacterial growth, analyzed by time-kill curves. However, the minimum inhibitory concentration and the minimum bactericidal concentration of GOCOOH-Ag were lower than those of GO-Ag for all strains studied, indicating that GOCOOH-Ag has better antibacterial activity. In addition, both nanomaterials prevent biofilm-formation, with a higher reduction of biofilm mass and cell viability in the presence of GOCOOH-Ag. The carboxylation functionalization in GO-based materials can be applied to improve the bactericidal and antibiofilm-forming action of the AgNPs.

Introduction

Infectious diseases caused by multidrug resistant microorganisms have become one of the most concerning threats to human health around the world[1]. The excessive use of antibiotics over years has led to the rise of drug resistant pathogens, resulting in poor treatment efficacy and significant economic loss. Alternatively, other antimicrobial agents for whom bacterial resistance is not expected have been used in order to overcome this problem. It is known that various metal ions and metallic oxides present antimicrobial activity against usual bacterial pathogens, although they are not exempt from the toxifying of normal human cells[2]. Likewise, quaternary ammonium salts have been widely used due to their excellent bactericidal properties[3],[4]; however, they can develop resistance in some bacterial strains after prolonged use[5]. On the other hand, topical antiseptics are effective antimicrobial agents for wound treatment, but repeated or inadequate applications may have negative results[6]. Other alternatives, such as pure antimicrobial peptides, have shown promising results; however they have a high production cost[7].

The advances of nanotechnology in the medicine field have contributed in recent years to the search for alternatives against the microbial resistance to traditional treatments. Due to their large specific surface area and unique properties, many nanoparticles (NPs) show antimicrobial behavior. Metal oxide NPs with

photocatalytic activity and capable of generating reactive oxygen species (ROS), such us TiO[8], CeO[9] or ZnO[10], have been studied. NPs of copper and its oxides represent some of the most explored compounds due to their broad range of bactericidal activity[11]. Nevertheless, silver nanoparticles (AgNPs) are the most used and tested in the biomedicine field, mainly due to their strong cytotoxicity and minimal resistance[12],[13],[14]. Despite of their outstanding properties, AgNPs also have some drawbacks, such as their tendency to form aggregates due to their high surface energy, which reduce their bactericidal activity[15].

Graphene-based nanomaterials have drawn much attention in the biomedical field due to their unique thermal, chemical and electric properties[16]. Some of the reported applications are for cellular imaging[17], nanocarriers in drug delivery[18], regenerative medicine[19] or bactericidal agents[20],[21],[22].

Combinations of graphene oxide (GO) with various biocidal materials, mainly metallic NPs have been explored, obtaining nanocomposites with significantly higher antibacterial activities[3],[23],[24]. Jizhen Ma *et al*.[25] modified the surface of GO sheets by depositing AgNPs and the hybrid material obtained showed an improved bactericidal effect, which was attributed by the authors to the synergistic effect produced by combining both materials.

Wangxiao He *et al*.[26] investigated the bactericidal activity of a TiO_2NPs-AuNPs-rGO composite against Gram-positive and Gram-negative bacteria and fungus. They found that the ternary composite material showed a higher antibacterial performance than rGO, TiO_2NPs, and TiO_2NPs-rGO did under solar light irradiation for 2 h, which was more effective toward Gram-positive bacteria than Gram-negative bacteria or fungi.

ZnO/GO composites were prepared by Yan-Wen Wang *et al*.[27], resulting in composites where ZnO NPs remained homogeneously anchored onto GO sheets. GO helped in the dispersion of ZnO NPs and enabled the intimate contact of *Escherichia Coli* with ZnO NPs and zinc ions as well. In addition, the ZnO/GO composites were found to be much less toxic to HeLa cells, compared to the equivalent concentration of ZnO NPs in the composites. The results showed that the synergistic effects of GO and ZnO NPs led to the superior antibacterial activity of the composites.

GO has a large specific surface area[28] and tends to form stable colloidal dispersions in water due to the hydrophilicity character provided for the oxygen-containing groups, such as hydroxyl, carboxyl, carbonyl, and epoxide, present on their surface[29]. These features make graphene highly biocompatible, thus making it an excellent substrate to generate new materials with bactericidal application[30],[31],[32]. Therefore, GO offers many possibilities for tuning their properties, through modifications on its oxygenated functional groups. Thereby, increasing the ratio of carboxyl groups distributed on the surface of the graphene oxide sheets is possible to achieve a more homogeneous deposition of the AgNPs. In turn, the presence of a greater number of carboxyl groups notably improves the dispersion of the material in water, while generating more stable dispersions that facilitate its bactericidal action.

In this work, carboxylated GO decorated with AgNPs (GOCOOH-Ag) was synthesized. The structural and morphological features of the obtained materials were studied by combining various techniques, such as scanning electron microscopy (SEM), transmission electron microscopy (TEM), ultraviolet-visible (UV-Vis) spectroscopy, Fourier-transform infrared spectroscopy (FTIR), X-ray diffraction (XRD) and X-ray photoelectron spectroscopy (XPS). Moreover, the antibacterial activity and antibiofilm-formation capacity were studied on a Gram+ and Gram- bacteria and further comparing with GO-AgNPs (GO-Ag) hybrid material prepared in the same conditions. Results showed that carboxylated material maximizes bactericidal activity and the biofilm-inhibition capacity of AgNPs against all strains tested in all range of the concentrations evaluated.

Experimental Part

Materials

Ultrathin graphite was provided by Avanzare S.L. (La Rioja, Spain). In addition, sulfuric acid (H_2SO_4, 95-98%), phosphoric acid (H_3PO_4, 85%), potassium permanganate ($KMnO_4$), hydrogen peroxide (H_2O_2, 30%), absolute ethanol (CH_3CH_2OH), chloroacetic acid ($ClCH_2COOH$), hydrocloric acid (HCl), sodium hydroxide (NaOH), sodium borohydride ($NaBH_4$) reagent grade were purchased from Alfa Aesar, Sigma Aldrich (Valencia, Spain), and used as received.

GO Synthesis

GO was synthesized from natural graphite by means of the improved Hummer's method[33]. A mixture of concentrated H_2SO_4/ H_3PO_4 (9:1 v:v) was added to a mixture of graphite powder and $KMnO_4$ (1:6 wt) in an ice bath and was later heated to 50°C, keeping this temperature under constant stirring for 12 h. The resulting product was cooled to room temperature and subsequently poured into ice water with H_2O_2 (30%). The mixture was sifted through a testing sieve (250 μm) and centrifuged (4000 rpm for 4 h), discarding the supernatant. The remaining solid material was then washed with 200 mL of water, 200 mL of 30% HCl, and 200 mL of ethanol, twice for each one. Once the multiple-wash process was finished, the remaining material was coagulated with 200 mL of ether and filtered with a 0.45 μm pore size membrane. The solid obtained on the filter was collected with deionized water and freeze dried under high vacuum.

GO-COOH Synthesis

Carboxylic acid-functionalized GO nanosheets (GOCOOH) were obtained through reaction with chloroacetic acid under strong basic conditions, in which the oxygen-containing groups of GO were converted to carboxylic groups[34]. Briefly, 1.2 g of Chloroacetic acid and 1 g of NaOH were added to 100 ml of a GO dispersion (0.5 mg/ml). The mixture was bath sonicated for 3 h at room temperature. The resulting solution was neutralized with HCl and then purified by repeated rinsing and filtration. The product obtained was finally redispersed and lyofilized.

GO-Ag and GOCOOH-Ag nanocomposites synthesis

Typically, 50 mg of GO were dispersed in 65 ml of water by ultrasonic bath treatment for 2 h. Then, 80 mg of $AgNO_3$ were added in the former dispersion on a magnetic stirrer to be mechanically mixed for 3 h. Next, 35 ml of a freshly prepared 0.1 M $NaBH_4$ aqueous solution was added drop by drop into the previously prepared solution and left under magnetic stirring for 6 h. The resulting dispersion was filtered and rinsed several times with deionized water. A GO-Ag nanocomposite was finally obtained by freeze drying. GOCOOH was subjected to the same process to get the GOCOOH-Ag nanocomposite.

Characterization

The UV–Vis absorption spectra were measured using JASCO V-670 spectrometer. The XRD measurements were performed on a 2D Phaser equipment (Bruker, Madrid, Spain), with Cu-Kα radiation working at 30 kV and 10 mA, in order to check the crystalline structure of the GO-based materials. Thermogravimetric analysis (TGA) was performed on a TGA Q50 thermogravimetric analyzer (TA Instruments, Cerdanyola del Valles, Spain). Samples (5–10 mg) were weighed in titanium crucibles and heated under a nitrogen atmosphere from 50 to 800°C at a heating rate of 10°C min^{-1}. The surface morphologies were obtained by SEM, (JSM 6300 JEOL, Tokyo, Japan) equipped with energy-dispersive X-ray spectrometer (EDS, Oxford Instruments, Bristol, UK) for elemental composition measurements. TEM images were acquired using JEM-1010 (JEOL DEBEN AMT, Tokyo, Japan). The presence of functional groups was assessed by means of FTIR. The FTIR spectra were acquired on a FT/IR-6200 (Jasco) spectrometer in the spectral window of 4000–400 cm^{-1} in ATR mode. The structure and composition of GO-based materials were studied by X-ray Photoelectron Spectroscopy (XPS) with a photoelectron spectrometer VG-Microtech Multilab 3000 (Thermo Fisher Scientific Inc., Waltham, MA, USA). Potential zeta was recorded using a dynamic laser scattering analyser (Zetasizer, 2000 HAS, Malvern, Worcestershire, UK).

Antibacterial activity

Antibacterial activity was ascertained by determining the minimum inhibitory concentration (MIC), minimum bactericidal concentration (MBC), time-killing curves and biofilm activity. MICs and MBCs were evaluated against four Gram-positive bacteria (*Staphylococcus aureus* V329[35] and ATCC25423; *Staphylococcus epidermidis* RP62A and ATCC32984) and two Gram-negative bacteria (*Pseudomonas aeruginosa* PFQ2 and *E. coli* ATCC25922). Strains V329, RP62A, PFQ2 and ATCC25922 are biofilm forming. Prior to analysis, each isolate was subcultured twice onto brain heart infusion (BHI, Scharlau) agar plates to ensure purity and viability of the test organism. Stock inoculum suspension was prepared by suspending 1 to 3 colonies in phosphate-buffered saline with a pH of 7.3 (PBS) from a 24 h culture and adjusted to a cell turbidity of 0.5 McFarland providing 1.5 x 10^8 CFU/ml. The density of inocula was confirmed by quantitative colony forming units (CFUs).

Firstly, a Kirby-Bauer plate diffusion method was performed to determine if GO and GOCOOH showed antibacterial activity by plating a 10 µl drop of a 10 mg/ml solution of GO materials onto Mueller-Hilton agar plates previously inoculated with the microorganism. After 24 h of incubation at 37 °C, the growth

inhibition zone was measured. All experiments measuring the antibacterial activity had a control that followed the same condition but without GO-Ag or GOCOOH-Ag.

MIC of GO-Ag and GOCOOH-Ag were determined by means of two-fold broth microdilution method using BHI as the culture medium and a final inoculum of 3×10^6 CFU/ml. The MICs were determined both visually and by spectrophotometer after 24 and 48 h of incubation and were defined as the lowest drug concentration, which completely inhibited growth. Concentrations of GO-Ag and GOCOOH-Ag tested ranged from 100 µg/ml to 0.1 µg/ml were obtained from a stock water solution of the nanohybrid of 200 µg/ml, which was sonicated for 5 min in an ultrasonic water bath. Further, two-fold dilutions were made in BHI. All concentrations of GO-Ag and GOCOOH-Ag are given in terms of Ag.

MBC was determined by transferring 0.1 ml from the clear (no growth) MIC wells onto BHI agar plates. Plates were incubated at 37°C for 24 h. The MBC was defined as the lowest drug concentration that killed ≥99.9% (≤ 10 colonies per plate) of bacteria.

Time-killing curves were evaluated in the presence of 12.66 µg/ml of GO-Ag or GOCOOH-Ag in a volume of 2 ml. The inoculum of cultures was set at 1.5×10^5 CFU/ml. Bacteria were incubated at 37 °C with agitation, and the number of CFU at selected time intervals (0, 1, 2, 3, 4, 6 and 24 h) was determined following the track-dilution method[36]. Briefly, aliquots of 0.1 ml of the cell suspension were serially ten-fold diluted up to 10^{-6} in a saline solution and 10 µl of various dilutions were spotted and track extended onto BHI agar plates. After 24 h incubation at 37°C, the number of CFU was determined. For each time and dilution, three replicates were performed. Assays were repeated on three different days.

The ability of GO-Ag and GOCOOH-Ag to prevent biofilm formation was quantified essentially as described elsewhere[37]. Biofilm was formed in a sterile flat-bottomed 96-well polystyrene microtiter plate (Sarstedt). Wells were filled with 200 µl of TSB supplemented with 0.25 wt% glucose (TSBG, Scharlau) and GO-Ag or GOCOOH-Ag at concentrations ranging from 50.62 to 0.1 µg/ml and 20 µl of the stock inoculum suspension, providing 3 x 10^6 CFU/ml. After 48 h of incubation at 37 °C, the wells were gently washed three times with 200 µl sterile PBS, air-dried in an inverted position, and stained with 0.1 % safranin for 30 s. The wells were rinsed and air-dried again, and the quantification of biofilm formed was determined by measuring the absorbance at 450 nm (Synergy H1 microplate reader, BioTek). Each concentration was tested in quadruplicate and on three separate experiments.

The cells' viability in the biofilm in the presence of GO-based materials was determined by scanning confocal laser microscopy. Biofilms were formed on sterile flat-bottomed 24-well polystyrene plates (Sarstedt) equipped with sterile glass discs. Wells were filled with 1 ml of TSBG and inoculated with 20 µl of the stock inoculum suspension, providing 3 x 10^6 CFU/mL, and then incubated for 24- 48 h at 37 °C. Then, glass discs were washed three times with 500 µl of sterile PBS to remove planktonic cells and stain with the LIVE/DEADTM BacLightTM bacterial viability kit (Thermo Fisher Scientific), following the manufacturer's instructions. This stain contains SYTO®9 and propidium iodide that, in a suitable mixture,

allow the visualization of viable bacteria (with an intact membrane), stained with green fluorescence and non-viable bacteria (with a compromised membrane) stained with red fluorescence.

All experiments of this section were performed in triplicate and on three separate days to ensure reproducibility. Results were expressed as mean ± SD.

Results And Discussion

Characterization of materials

A carboxylation procedure was applied to the parent GO with the aim of improving the AgNPs deposition process by achieving a more homogeneous decoration on the surface and avoiding the problems related to its aggregation, which is highly desirable for the bactericidal response of the material.

Morphology of the GO-based nanomaterials decorated with AgNPs was studied by TEM and shown in Figure 1. TEM micrographs (Figures 1a-c) reveal a homogeneous dispersion, with few aggregations, of spherical-like AgNPs decorating the sheets of GO-based materials. The EDS mapping shown in Figure 1(d) reveals the presence of AgNPs covering GOCOOH sheets. These results confirm the role of GO in the nucleation process and deposition of AgNPs, through strong interactions established between Ag+ ions and the oxygen-containing functional groups on the material surface. In the case of GOCOOH-Ag, the average size of the AgNPs was 6.74±0.25 nm against 11.69±4.82nm found for GO-Ag. In fact, 86% of the counted AgNPs on GOCOOH sheets were less than 10 nm in diameter. This narrow size distribution can be explained by both the strong reducing effect of borohydride and the stabilizing role of carboxylic groups, which allow the formation of smaller and better-distributed AgNPs for GOCOOH than for GO.

The UV–Vis spectrum of GO shown in Figure 2(a) exhibits a main absorption peak centered at 230 nm, which corresponds to the electronic π-π* transitions of C-C aromatic bonds, and a shoulder at 300 nm, associated to the n– π* transitions of C=O bonds[38]. A new band at 408 nm for GO-Ag and 405 nm for GOCOOH-Ag, corresponding to a surface plasmon of AgNPs, was observed, thus confirming the deposition of AgNPs on the GO-based material surface. Moreover, the symmetrical shape of the UV-Vis absorption peak, and its position, indicates a relatively narrow size distribution of small silver AgNPs[39].

Figure 2(b) shows the XRD patterns recorded for GO-Ag and GOCOOH-Ag nanomaterials. The presence of AgNPs on the GO-based nanosheet surface was confirmed by peaks at 2Θ values of about 38.1◦, 44.3◦, 64.5◦ and 77.5◦, which are assigned to the (1 1 1), (2 0 0), (2 2 0) and (3 1 1) crystallographic planes of face-centered cubic (fcc) AgNPs, respectively [JCPDS card No. 07-0783]. A sharp diffraction peak at 11.3□ for GOCOOH and 10.3□ for GO (Fig. 1 SI) was indexed to the (002) plane. For both silver decorated nanomaterials, this peak was slightly shifted to a greater angle, and a shoulder attributed to a hexagonal graphite structure appeared around 22□, indicating that the process carried out to incorporate AgNPs onto GO based materials induces a certain reduction on them, pointing out the partial restoration of the original graphitic order. Consequently, the intersheet distance decreases with the silver functionalization. In the case of GO, this value has a greater change than in GOCOOH, going from 0.86 to 0.74 Å, when GO

is decorated with AgNPs, compared with GOCOOH, where the distance between the adjacent planes decreases from 0.79 to 0.73 Å. Also, both GO-Ag and GOCOOH-Ag nanomaterials present a similar intersheet distance around 0.74 Å.

TGA measurements were conducted to characterize GO and GOCOOH and their AgNP nanohybrids, and the results are shown in Figure 3. All materials showed an initial weight decrease up to 100 °C due to the removal of adsorbed water[40]. This loss of weight is similar in GO and GOCOOH, which are smaller for AgNP-decorated GO-based nanomaterials, because the AgNPs deposition process induces a certain degree of reduction on the GO surface, increasing their hydrophobicity[41]. For GO and GOCOOH, oxygen-containing functional groups start their decomposition at 188 and 149 °C, respectively, indicating the greater presence of carboxyl groups onto the GOCOOH surface, which tend to decompose at lower temperatures[42]. When the temperature is increased above this point, a weight loss attributed to the decomposition of the more stable oxygen functionalities is observed for both materials[43]. Incorporation of AgNPs enhanced the thermal stability for GO-Ag and GOCOOH-Ag, indicating the participation of the oxygen functional groups on the AgNPs deposition process[44]. Furthermore, the final residual mass is more significant in AgNP-decorated GO-based nanomaterials, particularly in GOCOOH-Ag, which displayed the highest amount, attributed to the remaining GO carbon skeleton, as well as to AgNPs[45]. Therefore, the results obtained by TGA showed that carboxyl groups play an important role in the silver-decorating process.

The typical peaks related with the surface functional groups of GOCOOH and GOCOOH-Ag were displayed in the FTIR spectra as shown in Figure 4. The signal corresponding to carboxylic groups (C=O) was recorded at 1716 cm^{-1}. The peaks at 3433 cm^{-1}, associated with OH-group stretching, and at 1384 cm^{-1} associated with the deformation vibration of C–OH, were observed for both graphene oxide-based materials studied. The band at 1234 cm^{-1} was associated with the presence of the epoxide groups (C–O–C). Moreover, the C-O stretching appeared at 1058 cm^{-1} and the peak at 1612 cm^{-1} were attributed to the skeletal vibration of graphitic skeleton[46],[47]. After the functionalization with AgNPs, the peaks corresponding to the oxygen functional groups showed a decrease in intensity, which indicate the participation of the oxygen groups in the silver-reduction and functionalization process[48]. GO and GO-Ag (Figure 2 SI) showed the same trend, but a broad band in the C-OH stretching band region was observed for GO-Ag, due to some quantity of water molecules absorbed onto their surface.

Figure 5 shows the XPS spectra used to characterize the surface composition of the GO-based materials and their Ag-decorated hybrid materials. The C1s spectrum for GO (Figure 5a) shows several peaks at 284.60, 285.12, 286.84 and 288.49 eV attributed to the C–C, C=C, C–O and O–C=O groups, respectively[49]. The intensity of the O–C=O peak increased after the functionalization (Figure 5b), indicating the successful carboxylation of GO[50]. However, the decrease of the C–O related peakand the increase of the C=C peak confirmed a slight partial reduction of the GO during the carboxylation process, as seen by XRD analysis.

GO-Ag (Figure 5c) and GOCOOH-Ag (Figure 5d) showed in both cases a clear decrease in the intensity of the signal associated with the carboxyl groups, (i.e., around 288.5 eV). This decrease was more intense for the compound based on GOCOOH than for the one based on GO.

The presence of signals at 368.3 and 374.3 eV due to Ag $3d_{3/2}$ and Ag $3d_{5/2}$ (Figures 5e,f) suggests the formation of AgNPs onto GO and GOCOOH nanosheets. Moreover, the splitting of the 3d doublet of Ag is 6.0 eV, indicating the formation of metallic silver[51]. The XPS results, along with the above XRD and TEM results, clearly indicate that the AgNPs are well assembled on GO-based composites.

The results obtained by XPS measurements can be explained assuming that the carboxylic acid, hydroxyl or epoxide groups on the GO surface can act as nucleation sites for growth of the AgNPs and their further deposition onto GO sheets. Silver cations can be preferably attached to ionizable carboxylic functionalities, favoring the deposition process onto the exfoliated GOCOOH sheets through $NaBH_4$ reduction.

Zeta potential measurements were carried out with the aim to further study the carboxylic acid groups' role in the AgNPs deposition onto GO-based materials as well as to investigate their stability in water. Zeta potentials of GO, GOCOOH and hybrid solutions, GO-Ag and GOCOOH-Ag, were recorded at a pH of 6.0. Water suspension of GO exhibited a zeta potential of −39.6 mV similar to that of GOCOOH, whose value was −40.3 mV, due to the negatively charged surfaces caused by the presence of oxygen functional groups such as hydroxyl, epoxide and carboxylic.

Functionalization of hybrid materials with AgNPs caused a decrease in the Zeta potential values, yielding −35.9 mV for GO-Ag and −31.9 mV for GOCOOH-Ag. This decrease was more pronounced for the carboxylated product, indicating the participation of these groups in a preferential way in the deposition process of the NPs on the surface of the material[52], thus allowing GOCOOH-Ag to present a higher concentration of AgNPs than GO-Ag. The range of values obtained, all of them negatively charged, indicates a good stability in an aqueous solution for the GO and GOCOOH compounds: slight improvement for the carboxylated material and a moderate but sufficient stability for the Ag-decorated nanohybrids.

Antibacterial activity

Although several studies have reported that pristine GO presents antibacterial activity by itself[53],[54],[55], the Kirby-Bauer diffusion technique showed that neither GO nor GOCOOH exhibited zone inhibition, demonstrating the absence of antibacterial activity (Figure 3 SI). We attribute this fact to the variability of the GO-based materials, which can be influenced by many kinds of factors, such as the original graphite used for the GO synthesis, the different methods followed for the oxidation required to obtain the graphite oxide, the sonication step usually employed to separating the GO stacked sheets into individual sheets, the laborious filtration and drying process or even the time and conditions in which the material has been stored, which can also alter its properties. On the other hand, GO-based materials can avoid the AgNPs aggregation. In this sense, many reports have established that AgNPs improve their antibacterial activity

when they are deposited onto GO-based materials[25],[48],[56]. Therefore, further characterization was carried out with GO-Ag and GOCOOH-Ag materials.

As shown in Table 1, MIC and MBC of GOCOOH-Ag were lower than those of GO-Ag for all strains studied, indicating that GOCOOH-Ag has better antibacterial activity. The lowest 24 h MIC of GOCOOH-Ag was 3.16 µg/ml for *S. aureus* V329, whereas GO-Ag, in the same conditions, was 5.2 times greater. *S. epidermidis* RP62A and *E. coli* ATCC25922 were more resistant requiring 12.66 µg/ml of GOCOOH-Ag to be inhibited *versus* 32.92 and 16.46 µg/ml of GO-Ag, respectively. The 48 h MBC/MIC ratios of GOCOOH-Ag were ≤2 for all species tested (except *S. epidermidis* RP62A, which was >2), which is related to a bactericidal activity[57]. MBC/MIC ratio of GO-Ag was >2 for *S. aureus*, suggesting bacteriostatic activity and ≤2 for the other strains.

Table 1
MIC and MBC (µg/ml) of GO-Ag and GOCOOH-Ag values for all strains studied

Species	**Strains**	**GO-Ag**			**GOCOOH-Ag**		
		MIC		MBC	MIC		MBC
		24 h	48 h	48 h	24 h	48 h	48 h
S. aureus	ATCC 25423	16.46	16.46	65.85	6.33	12.66	25.31
S. aureus	V329	16.46	16.46	65.85	3.16	12.66	25.31
S. epidermidis	ATCC32984	16.46	32.92	65.85	6.33	12.66	25.31
S. epidermidis	RP62A	32.92	32.92	65.85	12.66	12.66	50.62
P. aeruginosa	PFQ2	32.92	32.92	65.85	6.33	12.66	12.66
E. coli	ATCC25922	16.46	32.92	65.85	12.66	12.66	12.66

The bactericidal action, determined by time-killing studies, was found to be dependent on both species and nanomaterial. The time-killing curves showed that 12.66 µg/ml of GO-Ag and GOCOOH-Ag reduced the bacterial growth with respect to the growth control of all strains tested. The killing activity of GOCOOH-Ag was very fast against *P. aeruginosa*, killing 100% of cells in 3 h (Figure 6). Against *E. coli*, GOCOOH-Ag required 5 h to kill 99.9% of cells and 6 h against *S. aureus*. However, no killing activity against *S. epidermidis* was observed, and the growth was always under the growth control (Figures 6 and 4 SI). In contrast, with the same concentration of GO-Ag, there was a slight killing (decrease in viable cells) in the first 6 h followed by an increase in viable cells but always below the control. The greatest CFU reduction at 24 h, with respect to the growth control, ranged between 1 and 2 Log depending on the strain.

From the MIC, MBC and time-killing study results, it can be concluded that the antimicrobial activity of AgNPs is considerably enhanced when they are loaded onto the GOCOOH surface.Activity of GO-based nanomaterials on biofilm formation was tested against two Gram positive (V329 and RP62A) and one Gram negative (PFQ2) bacteria, all of them with a high biofilm-forming capacity and a Gram-negative strain (ATCC 25922), which presents a low tendency toward biofilm formation.

Figures 7 and 5 SI show the quantification and visualization of biofilm formed and stained with safranin. Both nanomaterials prevent biofilm formation depending on the strain and concentration tested. The highest inhibitions were obtained with GOCOOH-Ag, and the minimum concentration required to completely inhibit biofilm formation ranged between 6.33 and 12.66 µg/ml. By contrast, with GO-Ag the minimum concentration to inhibit biofilm formation was four times higher than that of GOCOOH-Ag for all species except *E. coli* ATCC25922, which was similar for the two nanomaterials. The fact that both nanomaterials showed similar activity against *E. coli* could be related to the lower biofilm-forming capacity of this strain; consequently, a lower AgNPs concentration could be required to prevent biofilm formation, showing a minimal concentration to inhibit a biofilm formation of 12.66 µg/ml in the presence of GO-Ag.

The viability assay, by means of confocal microscopy performed on biofilm developing on glass discs in the presence of Ag-decorated GO-based nanomaterials, showed a considerable reduction of both biofilm mass and viable bacteria in all species tested (Figures 8 and 6 SI). Overall, above 6.33 µg/ml of GOCOOH-Ag a total absence of bacteria was observed, confirming no biofilm formation. However, with the same concentration of GO-Ag, only a reduction in biofilm mass and cellular viability with respect to control was achieved.

Conclusions

The bactericidal and antibiofilm-forming activity of AgNPs decorating the synthesized GO and GOCOOH materials were evaluated by using five techniques. The activity of AgNPs as a bactericidal and antibiofilm-forming agent was observed in both materials. Furthermore, the efficiency of AgNPs greatly improved when they were deposited onto the GOCOOH surface. Morphological characterization reveals a homogeneous dispersion of AgNPs with a narrow size distribution, achieved by the greater amount of carboxyl groups present on the GOCOOH surface, which can act as nucleation sites for the AgNPs growth. In addition, the prepared GO-based hybrid materials were easily dispersible in water-generating stable dispersions. In summary, the results obtained in this work open the door to exploring new applications of GOCOOH-Ag material as a bactericidal and antibiofilm-forming agent in the nanomedicine field.

Declarations

Conflicts of interest

There are no conflicts to declare.

Author Contributions

Conceptualization, A.B. MA.T. and E.G.; methodology, A.B., O.S, MA.T. and E.G.; writing—original draft preparation, A.B., E.G., MA.T.; writing—review and editing, A.B. MA.T., JM.P., P.B and E.G.; investigation, A.B., O.S., JM.P., P.B., MA.T. and E.G. All authors consulted their results and have read, critically reviewed, and agreed to the final version of the manuscript.

Acknowledgements

This research was funded by Agència Valenciana de la Innovació (Valencian Regional Government) under the project INNEST00/19/002 and the Spanish Ministerio de Economía, Industria y Competitividad (project SAF2017-82251-R). The authors would like to thank Dra. MP Marín (Microscopy service of Medical Research Institute Hospital La Fe) for the confocal microscopy images.

References

1. Levy SB, Marshall B (2004) Antibacterial resistance worldwide: causes, challenges and responses. Nat Med 10:S122–S129. https://doi.org/10.1038/nm1145
2. Tang J, Chen Q, Xu L et al (2013) Graphene Oxide–Silver Nanocomposite As a Highly Effective Antibacterial Agent with Species-Specific Mechanisms. ACS Appl Mater Interfaces 5:3867–3874. https://doi.org/10.1021/am4005495
3. Ahamed M, AlSalhi MS, Siddiqui MKJ (2010) Silver nanoparticle applications and human health. Clin Chim Acta 411:1841–1848. https://doi.org/10.1016/J.CCA.2010.08.016
4. Zhisheng Chen C, Beck-Tan C, Dhurjati N P, et al (2000) Quaternary Ammonium Functionalized Poly(propylene imine) Dendrimers as Effective Antimicrobials: Structure–Activity Studies. Biomacromol 1:473–480. https://doi.org/10.1021/bm0055495
5. Zhang S, Ding S, Yu J et al (2015) Antibacterial Activity, in Vitro Cytotoxicity, and Cell Cycle Arrest of Gemini Quaternary Ammonium Surfactants. Langmuir 31:12161–12169. https://doi.org/10.1021/acs.langmuir.5b01430
6. Kümmerer K (2004) Resistance in the environment. J Antimicrob Chemother 54:311–320. https://doi.org/10.1093/jac/dkh325
7. Yeaman MR, Yount NY (2003) Mechanisms of Antimicrobial Peptide Action and Resistance. Pharmacol Rev 55:27–55. https://doi.org/10.1124/pr.55.1.2
8. Kikuchi Y, Sunada K, Iyoda T et al (1997) Photocatalytic bactericidal effect of TiO2 thin films: dynamic view of the active oxygen species responsible for the effect. J Photochem Photobiol A Chem 106:51–56. https://doi.org/https://doi.org/10.1016/S1010-6030(97)00038-5

9. Surendra TV, Roopan SM (2016) Photocatalytic and antibacterial properties of phytosynthesized CeO2 NPs using Moringa oleifera peel extract. J Photochem Photobiol B Biol 161:122–128. https://doi.org/https://doi.org/10.1016/j.jphotobiol.2016.05.019
10. Seil JT, Webster TJ (2011) Reduced Staphylococcus aureus proliferation and biofilm formation on zinc oxide nanoparticle PVC composite surfaces. Acta Biomater 7:2579–2584. https://doi.org/https://doi.org/10.1016/j.actbio.2011.03.018
11. Chen S, Guo Y, Chen S et al (2012) Facile preparation and synergistic antibacterial effect of three-component Cu/TiO2/CS nanoparticles. J Mater Chem 22:9092–9099. https://doi.org/10.1039/C2JM00063F
12. Kalishwaralal K, BarathManiKanth S, Pandian SRK et al (2010) Silver nanoparticles impede the biofilm formation by Pseudomonas aeruginosa and Staphylococcus epidermidis. Colloids Surfaces B Biointerfaces 79:340–344. https://doi.org/https://doi.org/10.1016/j.colsurfb.2010.04.014
13. Rai MK, Deshmukh SD, Ingle AP, Gade AK (2012) Silver nanoparticles: the powerful nanoweapon against multidrug-resistant bacteria. J Appl Microbiol 112:841–852. https://doi.org/https://doi.org/10.1111/j.1365-2672.2012.05253.x
14. Webster TJ, Seil I (2012) Antimicrobial applications of nanotechnology: methods and literature. Int J Nanomedicine. https://doi.org/10.2147/IJN.S24805
15. Yun H, Kim JD, Choi HC, Lee CW (2013) Antibacterial Activity of CNT-Ag and GO-Ag Nanocomposites Against Gram-negative and Gram-positive Bacteria. Bull Korean Chem Soc 34:. https://doi.org/10.5012/bkcs.2013.34.11.3261
16. Allen J, Tung MC, Kaner VB R (2009) Honeycomb Carbon: A Review of Graphene. Chem Rev 110:132–145. https://doi.org/10.1021/cr900070d
17. Liu K, Zhang J-J, Cheng F-F et al (2011) Green and facile synthesis of highly biocompatible graphene nanosheets and its application for cellular imaging and drug delivery. J Mater Chem 21:12034–12040. https://doi.org/10.1039/C1JM10749F
18. Liu J, Cui L, Losic D (2013) Graphene and graphene oxide as new nanocarriers for drug delivery applications. Acta Biomater 9:9243–9257. https://doi.org/https://doi.org/10.1016/j.actbio.2013.08.016
19. Duran N, Martinez D, Silveira C et al (2015) Graphene Oxide: A Carrier for Pharmaceuticals and a Scaffold for Cell Interactions. Curr Top Med Chem 15:. https://doi.org/10.2174/1568026615666150108144217
20. Liu S, Hu M, Helen Zeng T et al (2012) Lateral Dimension-Dependent Antibacterial Activity of Graphene Oxide Sheets. Langmuir 28:12364–12372. https://doi.org/10.1021/la3023908
21. Akhavan O, Ghaderi E (2012) Escherichia coli bacteria reduce graphene oxide to bactericidal graphene in a self-limiting manner. Carbon N Y 50:1853–1860. https://doi.org/https://doi.org/10.1016/j.carbon.2011.12.035
22. Hu W, Peng C, Luo W et al (2010) Graphene-Based Antibacterial Paper. ACS Nano 4:4317–4323. https://doi.org/10.1021/nn101097v

23. Hussain N, Gogoi A, Sarma RK et al (2014) Reduced Graphene Oxide Nanosheets Decorated with Au Nanoparticles as an Effective Bactericide: Investigation of Biocompatibility and Leakage of Sugars and Proteins. Chempluschem 79:1774–1784. https://doi.org/https://doi.org/10.1002/cplu.201402240
24. Akhavan O, Ghaderi E (2009) Photocatalytic Reduction of Graphene Oxide Nanosheets on TiO2 Thin Film for Photoinactivation of Bacteria in Solar Light Irradiation. J Phys Chem C 113:20214–20220. https://doi.org/10.1021/jp906325q
25. Ma J, Zhang J, Xiong Z et al (2011) Preparation, characterization and antibacterial properties of silver-modified graphene oxide. J Mater Chem 21:3350–3352. https://doi.org/10.1039/C0JM02806A
26. He W, Huang H, Yan J, Zhu J (2013) Photocatalytic and antibacterial properties of Au-TiO2 nanocomposite on monolayer graphene: From experiment to theory. J Appl Phys 114:204701. https://doi.org/10.1063/1.4836875
27. https://doi.org/10.1021/am4053317
28. Taylor E, Webster TJ (2011) Reducing infections through nanotechnology and nanoparticles. Int J Nanomedicine 6:1463–1473. https://doi.org/10.2147/IJN.S22021
29. Pasricha R, Gupta S, Joshi AG et al (2012) Directed nanoparticle reduction on graphene. Mater Today 15:118–125. https://doi.org/https://doi.org/10.1016/S1369-7021(12)70047-0
30. Liu Y, Huang J, Li H (2013) Synthesis of hydroxyapatite–reduced graphite oxide nanocomposites for biomedical applications: oriented nucleation and epitaxial growth of hydroxyapatite. J Mater Chem B 1:1826–1834. https://doi.org/10.1039/C3TB00531C
31. Xu C, Wang X, Zhu J (2008) Graphene–Metal Particle Nanocomposites. J Phys Chem C 112:19841–19845. https://doi.org/10.1021/jp807989b
32. Xu C, Wang X, Yang L, Wu Y (2009) Fabrication of a graphene–cuprous oxide composite. J Solid State Chem 182:2486–2490. https://doi.org/https://doi.org/10.1016/j.jssc.2009.07.001
33. Marcano C, Kosynkin DV, Berlin DM J, et al (2010) Improved Synthesis of Graphene Oxide. ACS Nano 4:4806–4814. https://doi.org/10.1021/nn1006368
34. Yu S, Liu J, Zhu W et al (2015) Facile room-temperature synthesis of carboxylated graphene oxide-copper sulfide nanocomposite with high photodegradation and disinfection activities under solar light irradiation. Sci Rep 5:16369. https://doi.org/10.1038/srep16369
35. Carme C, Cristina S, Jaione V et al (2001) Bap, a Staphylococcus aureus Surface Protein Involved in Biofilm Formation. J Bacteriol 183:2888–2896. https://doi.org/10.1128/JB.183.9.2888-2896.2001
36. Jett BD, Hatter KL, Huycke MM, Gilmore MS (1997) Simplified agar plate method for quantifying viable bacteria. Biotechniques 23:648–650. https://doi.org/10.2144/97234bm22
37. Tormo M, Knecht E, Götz F et al (2005) Bap-dependent biofilm formation by pathogenic species of Staphylococcus: evidence of horizontal gene transfer? Microbiology 151:2465–2475. https://doi.org/https://doi.org/10.1099/mic.0.27865-0

38. Li J, Liu C (2010) Ag/Graphene Heterostructures: Synthesis, Characterization and Optical Properties. Eur J Inorg Chem 2010:1244–1248. https://doi.org/https://doi.org/10.1002/ejic.200901048
39. Yin B, Ma H, Wang S, Chen S (2003) Electrochemical Synthesis of Silver Nanoparticles under Protection of Poly(N-vinylpyrrolidone). J Phys Chem B 107:8898–8904. https://doi.org/10.1021/jp0349031
40. Zhao L, Yang S-T, Feng S et al (2017) Preparation and Application of Carboxylated Graphene Oxide Sponge in Dye Removal. Int J Environ Res Public Health 14:. https://doi.org/10.3390/ijerph14111301
41. Shen J, Shi M, Li N et al (2010) Facile synthesis and application of Ag-chemically converted graphene nanocomposite. Nano Res 3:339–349. https://doi.org/10.1007/s12274-010-1037-x
42. Pruna AI, Barjola A, Cárcel AC et al (2020) Effect of Varying Amine Functionalities on CO2 Capture of Carboxylated Graphene Oxide-Based Cryogels. Nanomaterials 10:. https://doi.org/10.3390/nano10081446
43. Shen J, Li T, Shi M et al (2012) Polyelectrolyte-assisted one-step hydrothermal synthesis of Ag-reduced graphene oxide composite and its antibacterial properties. Mater Sci Eng C 32:2042–2047. https://doi.org/https://doi.org/10.1016/j.msec.2012.05.017
44. Kim K-S, Kim I-J, Park S-J (2010) Influence of Ag doped graphene on electrochemical behaviors and specific capacitance of polypyrrole-based nanocomposites. Synth Met 160:2355–2360. https://doi.org/https://doi.org/10.1016/j.synthmet.2010.09.011
45. Zhao R, Lv M, Li Y et al (2017) Stable Nanocomposite Based on PEGylated and Silver Nanoparticles Loaded Graphene Oxide for Long-Term Antibacterial Activity. ACS Appl Mater Interfaces 9:15328–15341. https://doi.org/10.1021/acsami.7b03987
46. Wang H-W, Hu Z-A, Chang Y-Q et al (2011) Design and synthesis of NiCo2O4–reduced graphene oxide composites for high performance supercapacitors. J Mater Chem 21:10504–10511. https://doi.org/10.1039/C1JM10758E
47. Pham VH, Cuong TV, Hur SH et al (2011) Chemical functionalization of graphene sheets by solvothermal reduction of a graphene oxide suspension in N-methyl-2-pyrrolidone. J Mater Chem 21:3371–3377. https://doi.org/10.1039/C0JM02790A
48. Cai X, Lin M, Tan S et al (2012) The use of polyethyleneimine-modified reduced graphene oxide as a substrate for silver nanoparticles to produce a material with lower cytotoxicity and long-term antibacterial activity. Carbon N Y 50:3407–3415. https://doi.org/https://doi.org/10.1016/j.carbon.2012.02.002
49. Liu Y, Tian C, Yan B et al (2015) Nanocomposites of graphene oxide, Ag nanoparticles, and magnetic ferrite nanoparticles for elemental mercury (Hg0) removal. RSC Adv 5:15634–15640. https://doi.org/10.1039/C4RA16016A
50. Pei F, Liu Y, Zhang L et al (2013) TiO2 nanocomposite with reduced graphene oxide through facile blending and its photocatalytic behavior for hydrogen evolution. Mater Res Bull 48:2824–2831. https://doi.org/https://doi.org/10.1016/j.materresbull.2013.04.018

51. Gunawan C, Teoh WY, Marquis CP et al (2009) Reversible Antimicrobial Photoswitching in Nanosilver. Small 5:341–344. https://doi.org/https://doi.org/10.1002/smll.200801202
52. Pasricha R, Gupta S, Srivastava AK (2009) A Facile and Novel Synthesis of Ag–Graphene-Based Nanocomposites. Small 5:2253–2259. https://doi.org/https://doi.org/10.1002/smll.200900726
53. Liu S, Helen Zeng T, Hofmann M et al (2011) Antibacterial Activity of Graphite, Graphite Oxide, Graphene Oxide, and Reduced Graphene Oxide: Membrane and Oxidative Stress. ACS Nano 5:6971–6980. https://doi.org/10.1021/nn202451x
54. Akhavan O, Ghaderi E, Esfandiar A (2011) Wrapping Bacteria by Graphene Nanosheets for Isolation from Environment, Reactivation by Sonication, and Inactivation by Near-Infrared Irradiation. J Phys Chem B 115:6279–6288. https://doi.org/10.1021/jp200686k
55. Veerapandian M, Zhang L, Krishnamoorthy K, Yun K (2013) Surface activation of graphene oxide nanosheets by ultraviolet irradiation for highly efficient anti-bacterials. Nanotechnology 24:395706. https://doi.org/10.1088/0957-4484/24/39/395706
56. Das MR, Sarma RK, Saikia R et al (2011) Synthesis of silver nanoparticles in an aqueous suspension of graphene oxide sheets and its antimicrobial activity. Colloids Surfaces B Biointerfaces 83:16–22. https://doi.org/https://doi.org/10.1016/j.colsurfb.2010.10.033
57. de Moraes ACM, Lima BA, de Faria AF et al (2015) Graphene oxide-silver nanocomposite as a promising biocidal agent against methicillin-resistant Staphylococcus aureus. Int J Nanomedicine 10:6847–6861. https://doi.org/10.2147/IJN.S90660

Figures

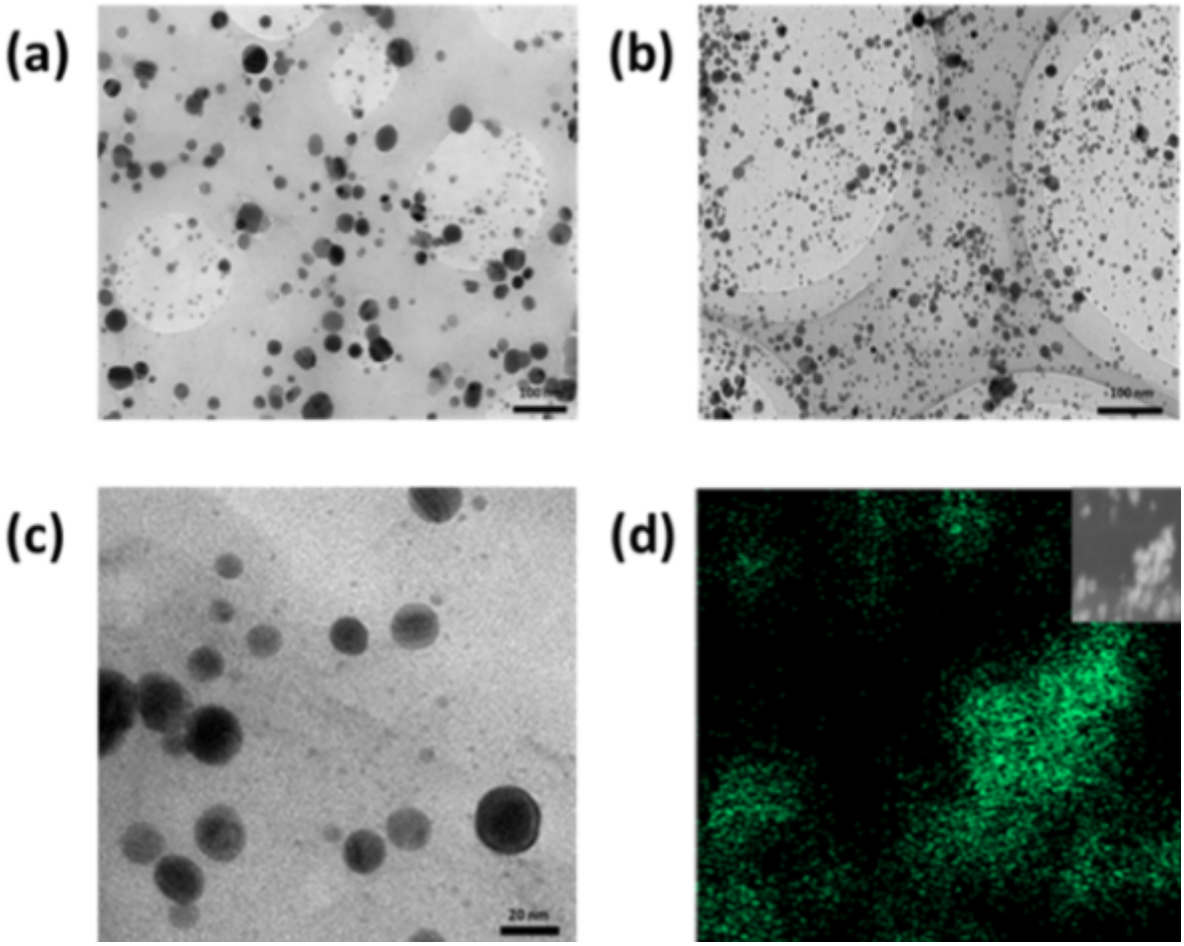

Figure 1

TEM micrographs of (a) GO-Ag; (b) GOCOOH-Ag; (c) magnified image of GOCOOH-Ag and (d) EDS mapping of AgNPs deposited on the GOCOOH surface.

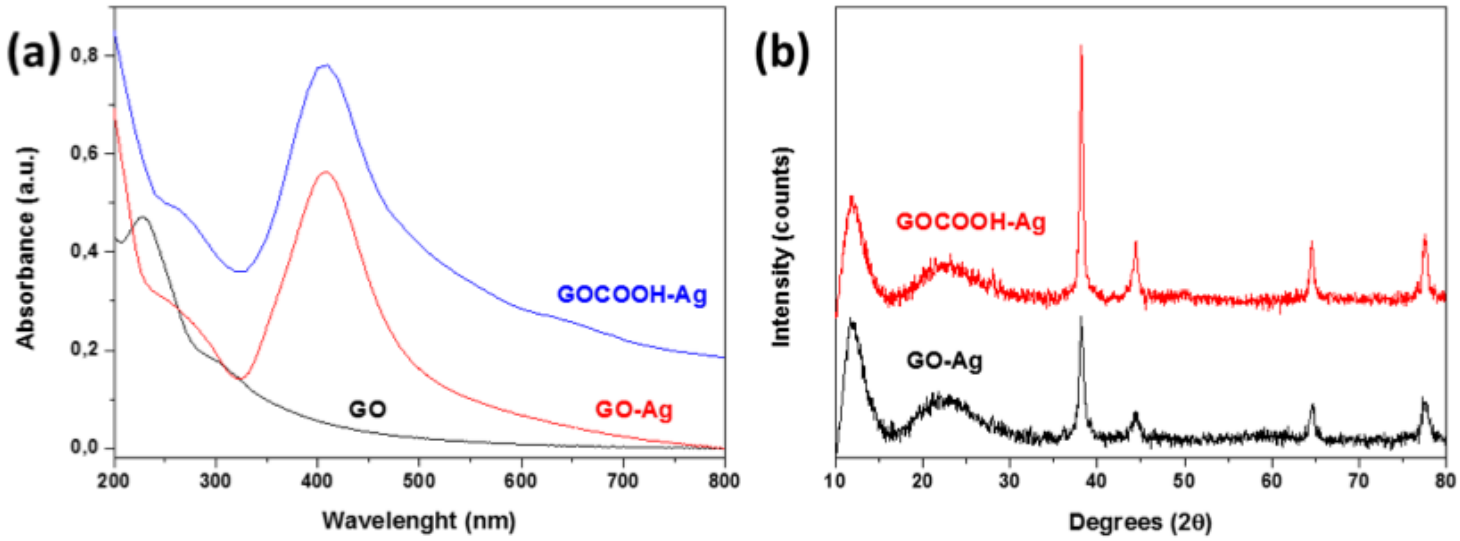

Figure 2

(a) UV–Vis absorption spectra of GO (black), GO-Ag (red) and GOCOOH-Ag (blue); (b) XRD spectrum for GO-Ag (black) and GOCOOH-Ag (red).

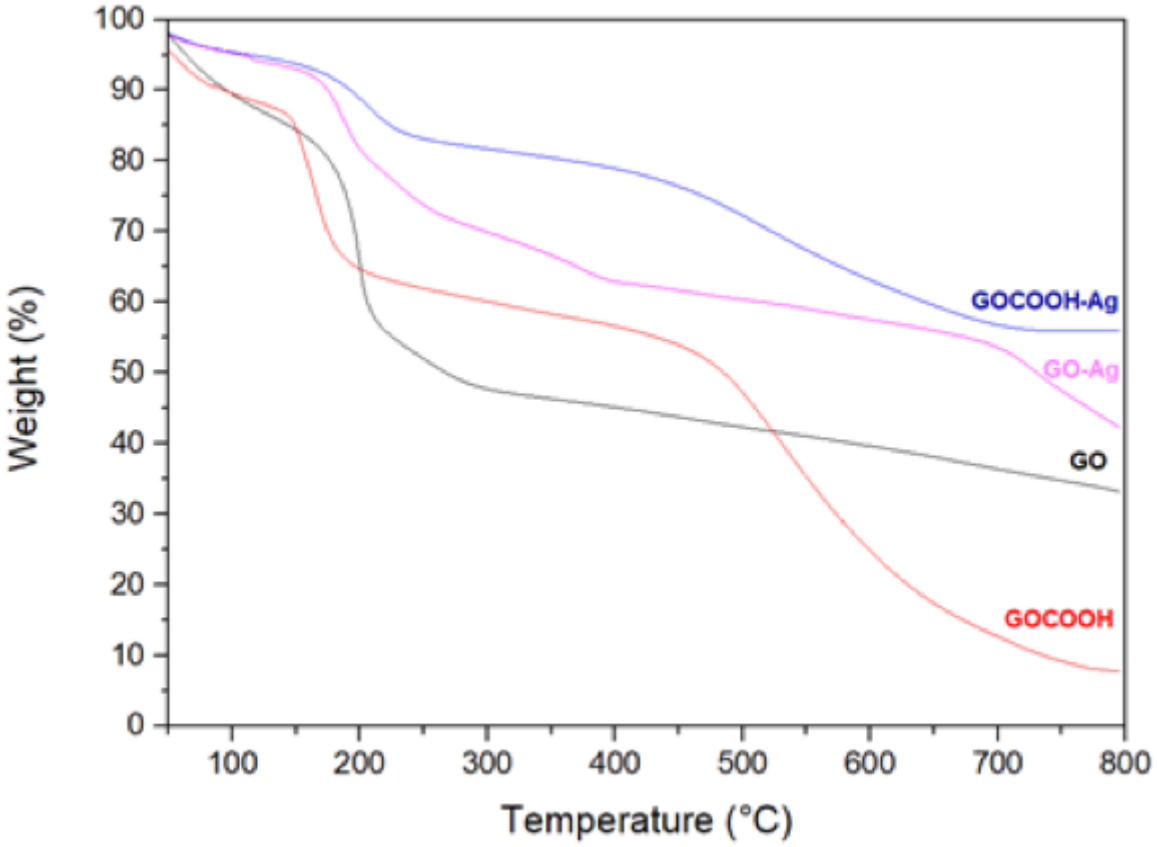

Figure 3

Thermogravimetric curves for GO, GOCOOH, GO-Ag and GOCOOH-Ag.

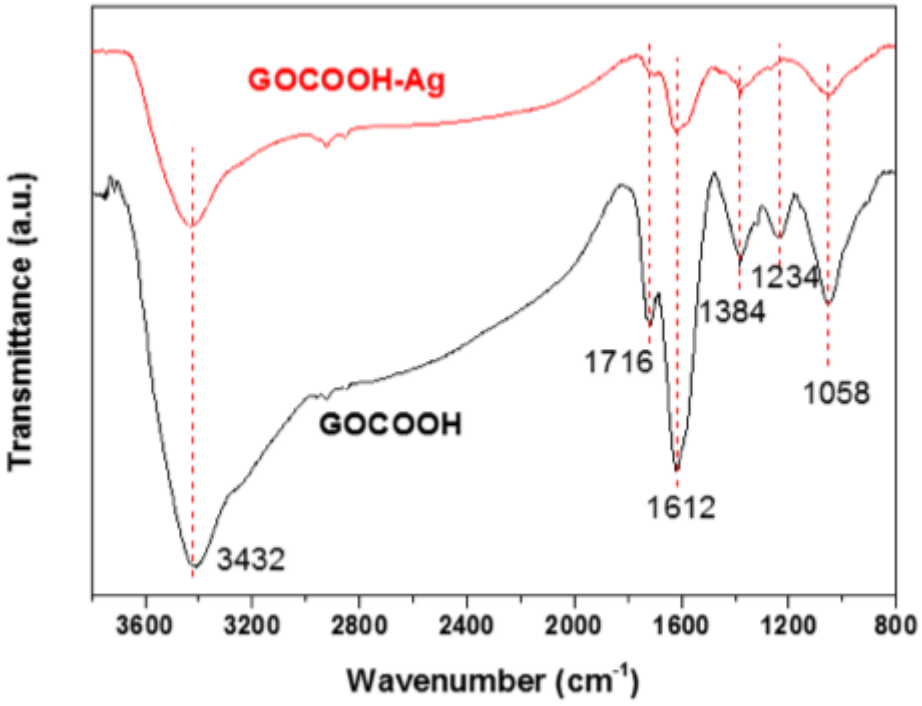

Figure 4

FTIR spectra for GOCOOH and GOCOOH-Ag.

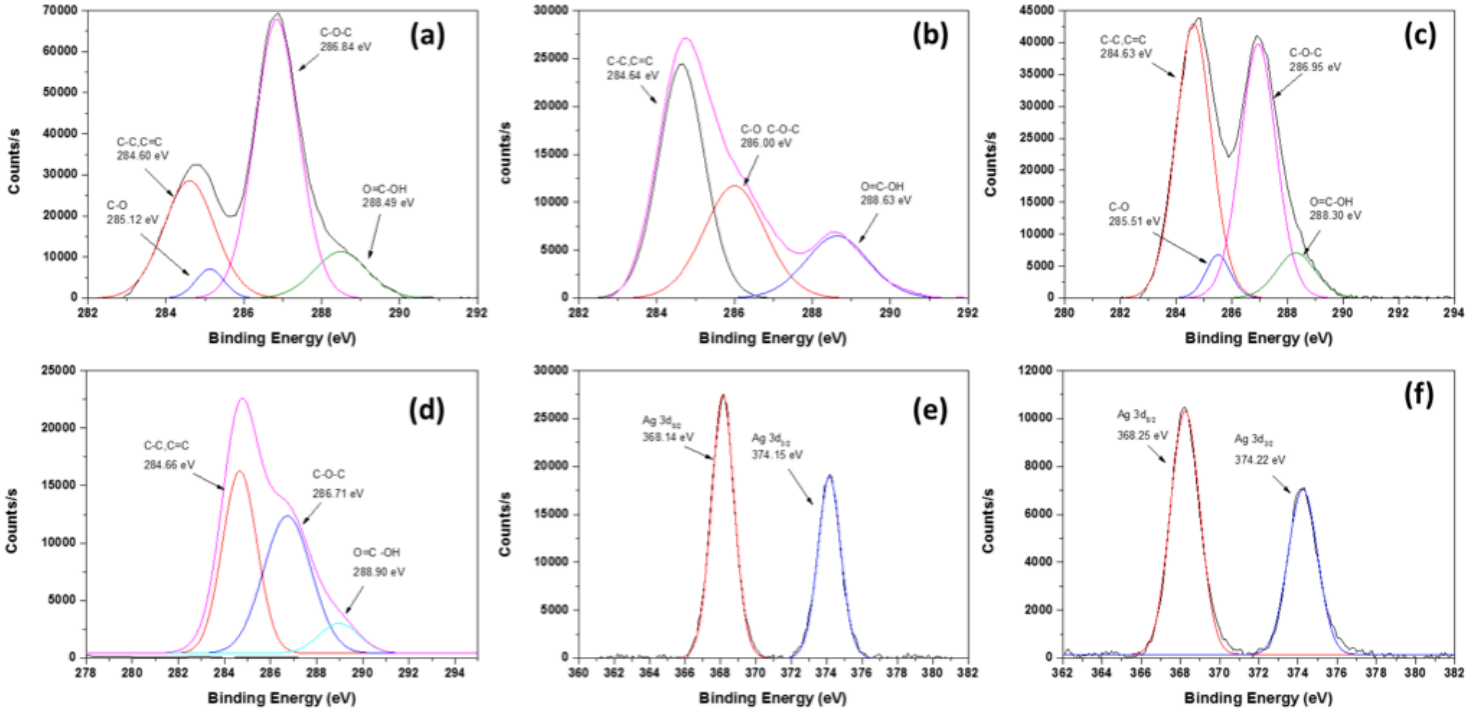

Figure 5

C1s XPS spectra deconvolution of (a) GO; (b) GOCOOH; (c) GO-Ag; (d) GOCOOH-Ag and (e) XPS patterns of Ag3d spectra for GO-Ag and (f) GOCOOH-Ag.

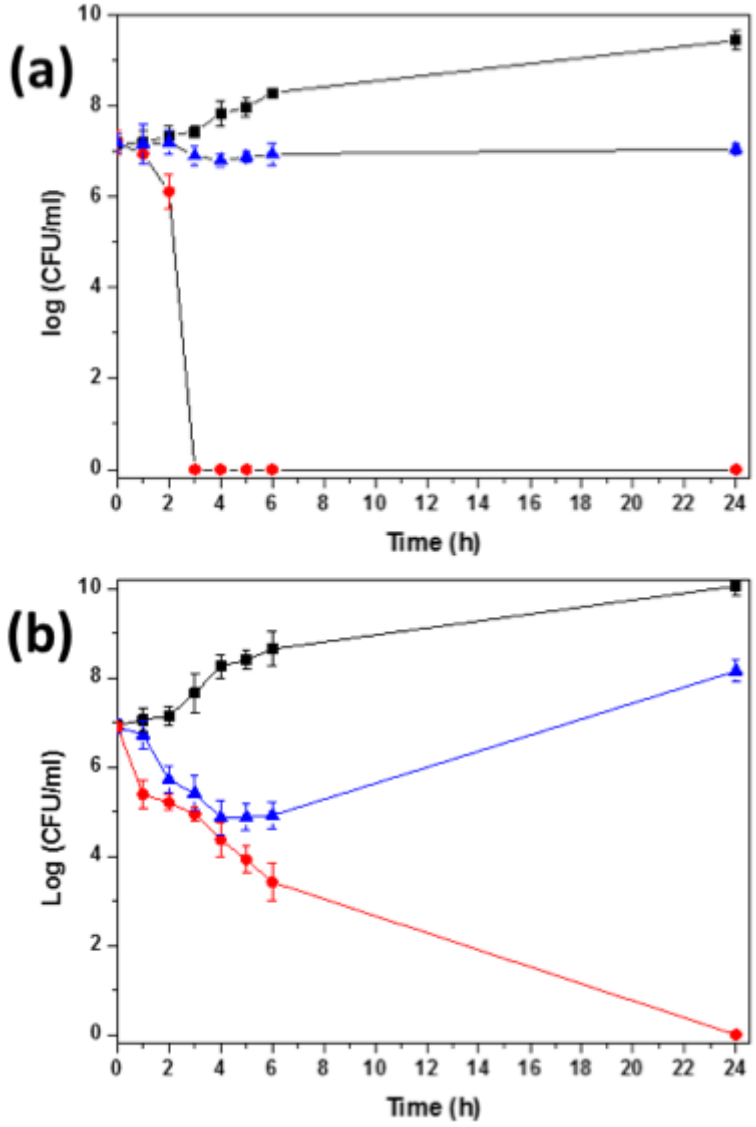

Figure 6

Time-killing curve of (a) P. aeruginosa (PFQ2) and (b) E. coli (ATCC25922) in the presence of GO-Ag and GOCOOH-Ag at 12.66 µg/ml. The data were presented as a means and SD of at least three independent experiments.

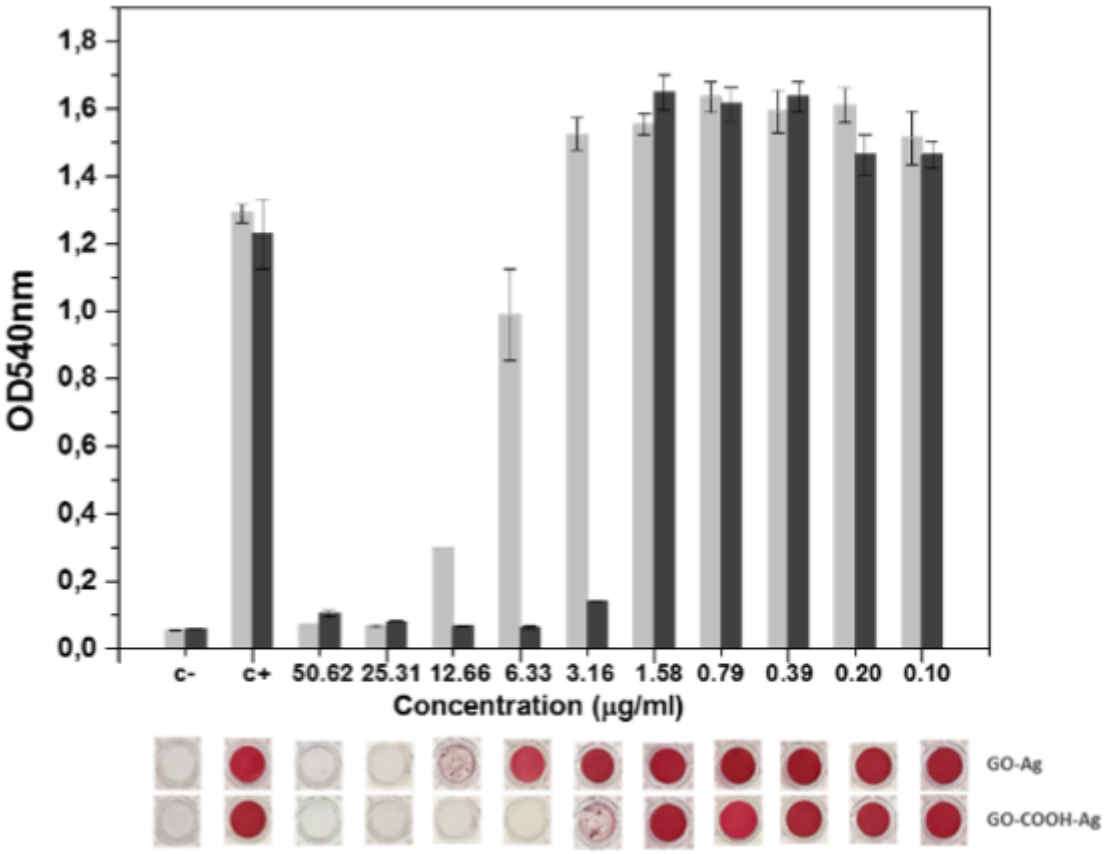

Figure 7

Effect of GO-Ag (light gray) and GOCOOH-Ag (dark gray) on the biofilm formation of S. aureus V329. Quantification (upper panel) and images (lower panel) of the biomass of a 48 h biofilm.

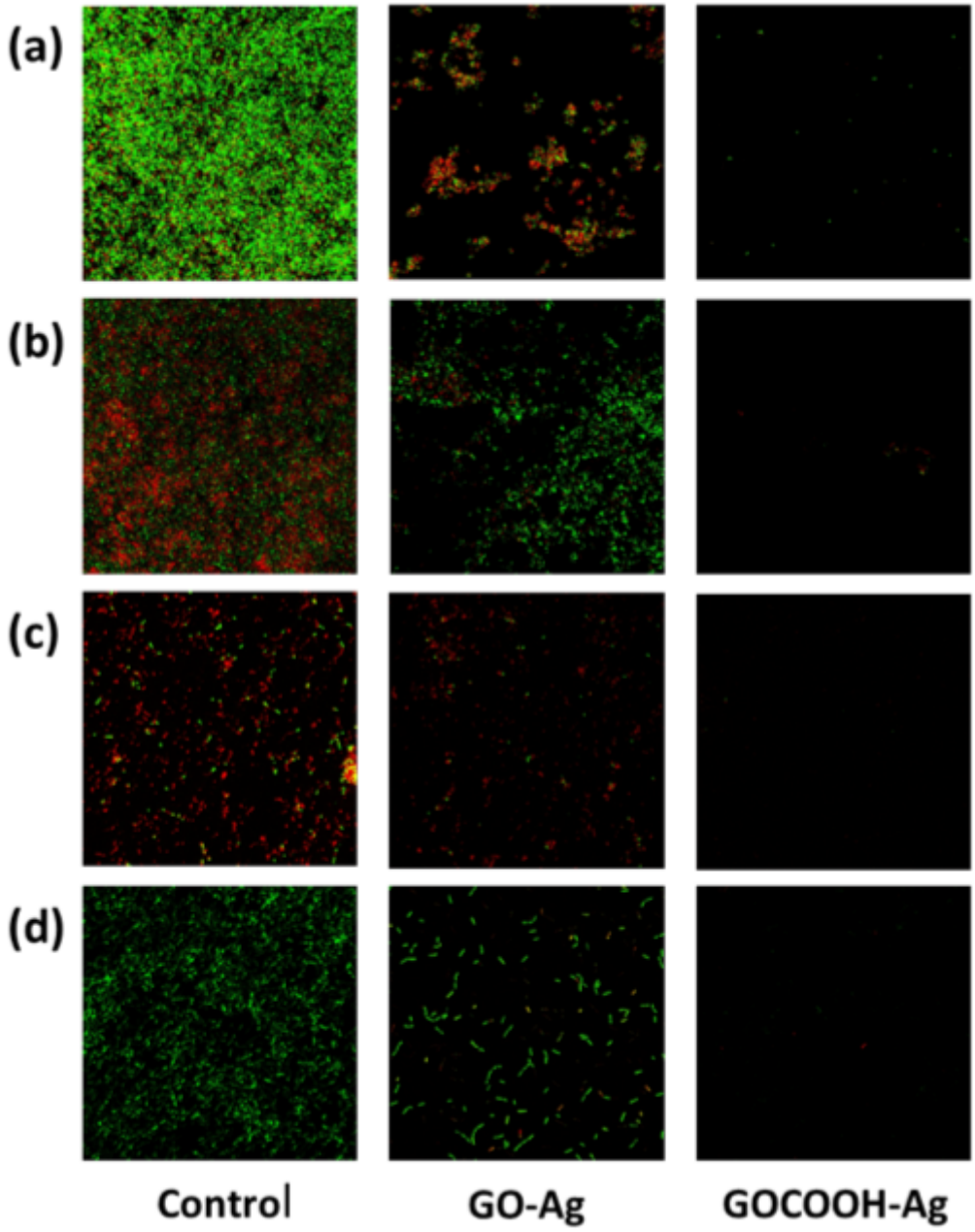

Figure 8

Confocal microscopy images biofilm of (a) S. aureus V329; (b) S. epidermidis RP62A; (c) P. aeruginosa PFQ2 and (d) E. coli ATCC25922. The bacteria were grown in TSBG for 48 h (control) with GO-Ag and GOCOOH-Ag at 6.33 µg/ml concentration.

Supplementary Files

This is a list of supplementary files associated with this preprint. Click to download.

- SupplInfoNanoscaleResearchLetters.docx